Theoretical and numerical estimates of the gas-liquid critical point of a primitive model for silica

Emanuela Bianchi,[1,a)] Piero Tartaglia,[1] and Francesco Sciortino[2]

[1]Dipartimento di Fisica and INFM-CRS-SMC, Università di Roma La Sapienza, Piazzale A. Moro 2, 00185 Roma, Italy

[2]Dipartimento di Fisica and INFM-CRS-SOFT, Università di Roma La Sapienza, Piazzale A. Moro 2, 00185 Roma, Italy

We present a numerical evaluation of the critical point location for a primitive model for silica recently introduced by Ford *et al.* [J. Chem. Phys. **121**, 8415 (2004)]. We complement the numerical estimate with a theoretical description of the system free energy (and related thermodynamic quantities) by solving (i) the standard parameter-free first order thermodynamic perturbation Wertheim theory and (ii) an *ad hoc* modeling of the temperature and density dependences of the bonding free energy, inspired by the Wertheim theory but requiring one fitting parameter $\alpha(\rho)$. This parameter takes into account the correlation between adjacent bonding induced by excluded volume effects. We compare the predicted critical point location in the temperature-density plane with the "exact" numerical Monte Carlo value. The critical temperature is correctly predicted by both theoretical approaches, while only approach (ii) is able to accurately predict the critical density. © *2008 American Institute of Physics.* [DOI: 10.1063/1.3023151]

I. INTRODUCTION

Recently Ford *et al.*[1] introduced a simple and computationally efficient primitive model of silica (PSM). This model aims to reproduce the key chemical and physical features of SiO_2, i.e., the strong association between bonded silicon and oxygen atoms and the low tetrahedral coordination of the oxygen atoms around a silicon atom. In the model, oxygen atoms are represented by bivalent particles and the silicon atoms are described by tetravalent ones. Both Si and O atoms are modeled as (nonadditive) hard sphere particles decorated by four and two short-range bonding "sticky" sites, respectively. The bonding sites are located at fixed distances from the particle centers and arranged in such a way that the tetrahedral coordination of oxygen particles around a single silicon particle is reproduced. Despite the absence of long-range forces, the numerically calculated phase diagram and the mechanical properties of silica most common solid phase structures, such as cristobalite, quartz, and coesite, reproduce quite accurately the experimental results. The good qualitative agreement with experimental data on the dense silica phases[1] validates the PSM as a powerful and simple model for silica. The same model has also been used to study the phase stability of zeolite frameworks[2] as well as the dynamic properties of the fluid phase, with a particular emphasis in the region where bonding (as opposed to caging) slows down the dynamics near to a dynamic arrest transition.[3] From the initial observation of Ford *et al.*[1] and the numerical estimates reported in Ref. 3, it appears that in this model a liquid phase is technically missing since no critical point is observed in the region where the fluid is the stable phase. The disappearance of the stable gas-liquid critical point in the equilibrium phase diagram is probably associated with the short-range nature of the attractive interaction of the model, in analogy with the behavior of spherical interacting potentials in the limit of short attractive ranges.[4–7] Nevertheless, the critical point can still be observed in metastable conditions, i.e., when the typical time scale of crystallization is significantly longer than the observation time scale.[8,9] Determining the existence and the temperature-density location of the critical point allows a deeper understanding on the behavior of the system. Indeed, if the gas-liquid critical point lies in the fluid-solid coexistence region, like for other primitive patchy models,[10] the liquid phase is not observed as an equilibrium stable phase but only in a metastable condition.

In this article we report a precise estimate of the location of the critical point for the PSM, resulting from grand canonical simulations and histogram reweighing techniques.[11–13] We complement the numerical evaluation with two theoretical approaches: (i) we solve the Wertheim theory (WT) for associating liquids, providing a parameter-free prediction for the model free energy, and (ii) we modify the Wertheim expression for the bonding chemical equilibrium to incorporate, at zeroth order level, the correlation between adjacent bonds induced by excluded volume interactions. In this second case, the resulting free energy provides a rather good description of the temperature and density dependences of the bond probability. The theoretical critical points are also compared to the numerical evaluation of the critical temperature T_c and density ρ_c. Both theoretical approaches correctly predict T_c but only the second one is able to accurately estimate ρ_c.

a)Electronic mail: emanuela.bianchi@roma1.infn.it.

II. THE MODEL

The primitive model for silica consists of a binary mixture of patchy particles with different valences. The mixture of Si and O (in a 1:2 ratio) is a nonadditive hard sphere mixture. More precisely, the Si–Si and Si–O nonbonded interactions are hard core repulsions with hard sphere diameter $\sigma_{SiSi} = \sigma_{SiO} \equiv \sigma$ (where σ defines the length scale), while the O–O hard core is defined by $\sigma_{OO} = 1.6\sigma$. The four attractive sites of silicon are arranged in a tetrahedral geometry and located on the hard core surface, i.e., at a distance of 0.5σ from the particle center. The two oxygen bonding sites are located at a distance of 0.5σ from the particle center and the angle between them is fixed at 145.8°. The only attractive interaction takes place between pairs of Si and O sites. Sticky sites interact via a square well potential of depth $-u_0$ for $r \leq \delta$ and 0 otherwise. When the interaction takes place between an oxygen and a silicon particle, the potential $V(1,2)$ between particles 1 and 2 is given by

$$V(1,2) = V_{HS}(\mathbf{r}_{12}) + \sum_{i=1}^{4} \sum_{j=1}^{2} V_{SW}(\mathbf{r}_{12}^{ij}), \tag{1}$$

where V_{HS} is the hard sphere potential and V_{SW} is the site-site square well interaction. Here $\mathbf{r}_{12}$ and $\mathbf{r}_{12}^{ij}$ are the vectors joining the particle-particle and the site-site (on different particles) centers, respectively. The individual sites are denoted by i (site on the Si particle) and j (site on the O particle). When the interaction takes place between particles of the same type, only the repulsive contribution [first term in the right hand side of Eq. (1)] survives. The attractive interaction range is chosen to be $\delta = (1 - \sqrt{3}/2)\sigma \approx 0.134\sigma$, a value for which double bonding at the same site is not observed, as discussed in Ref. 3. In this model, bonding is properly defined: two particles are considered bonded when their interaction energy is equal to $-u_0$ (where u_0 defines the energy scale). Hence, the potential energy is a precise measure of the number of bonds present in the system. Temperature is measured in units of the potential depth (i.e., Boltzmann constant $k_B = 1$).

We note that the nonadditivity of the mixture has a direct influence on the O–Si–O bonding. As we show in Sec. IV, some O–Si–O angular configurations are incompatible with three-particles bonding since two oxygens bonded to the same silicon particle interact via the nonadditive hard core repulsion (see Fig. 1). The features of the model thus introduce a correlation between adjacent bonding sites. Indeed, if a silicon particle is bonded to an oxygen one, a second oxygen approaching the bonded dimer would be partially hindered in bonding to the same silicon (in any of the remaining free sites) by the presence of the first bonded oxygen.

III. MONTE CARLO SIMULATIONS

To estimate the location of the gas-liquid critical point in the temperature-density plane, we perform standard Monte Carlo simulations in the grand canonical ensemble (GCMC). In this ensemble, the chemical potential μ, the temperature
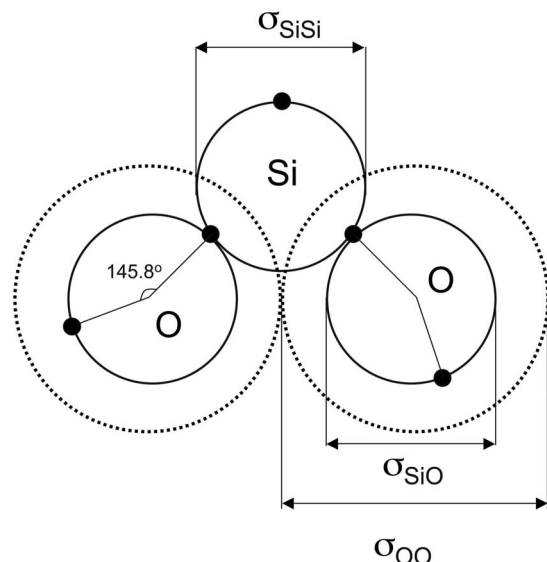

FIG. 1. Two dimensional (2D) schematic representation of the O–Si–O bonding geometry. The Si–Si and Si–O hard core interactions have diameters of $\sigma_{SiSi} = \sigma_{SiO} \equiv \sigma$, while the O–O hard core diameter is $\sigma_{OO} = 1.6\sigma$. Black points on the spheres represent the bonding sites. Silicon has four attractive sites arranged in a tetrahedral geometry (in the 2D figure only three of them are visible) and located at a distance of 0.5σ from the particle center. The two oxygen bonding sites are located at a distance of 0.5σ from the particle center and the angle between them is 145.8°.

T, and the volume V are fixed. MC moves include insertion and deletion of particles as well as particle translation and rotations. A MC step is defined as 50 000 attempts to perform displacement moves and 100 attempts to insert or delete a particle (with equal probability of being Si or O). In the displacement moves, a particle is randomly translated by a random quantity between $\pm 0.05\sigma$ in each direction and rotated around a randomly chosen angle by a random quantity between ± 0.5 rad. We perform simulations at fixed V, T, μ_1, and μ_2 (where μ_1 and μ_2 are the chemical potentials of the two species of the mixture), and we tune T, μ_1, and μ_2 until the simulated system shows ample density fluctuations, signaling the proximity to the critical point. Once a reasonable guess of the critical point in T, μ_1, and μ_2 is reached, we start 15 independent GCMC simulations to improve the statistics of the fluctuations of the number of particles N in the box and of the potential energy E. We note that since the critical temperature is found to be around $T \sim 0.075$, the probability of breaking a bond $\sim e^{1/T}$ is extremely small and hence numerical simulations are particularly time consuming. Each independent realization of the system was simulated for 10^7 MC steps, corresponding to about 20 days in a 3.4 GHz processor. We have studied different sizes and report the values for the largest one, corresponding to a box of side $L = 9\sigma$. In these conditions, the total number of particles in the simulated box oscillates between 0 and 160, as shown in Fig. 2. Figure 2 also shows the number of particle distribution $P(N)$ at the studied T closest to the critical temperature.

The precise location of the critical point is obtained through a fitting procedure associated with histogram reweighing.[11] This technique allows us to predict the distribution of N at T', μ_1', and μ_2' within few percents of the
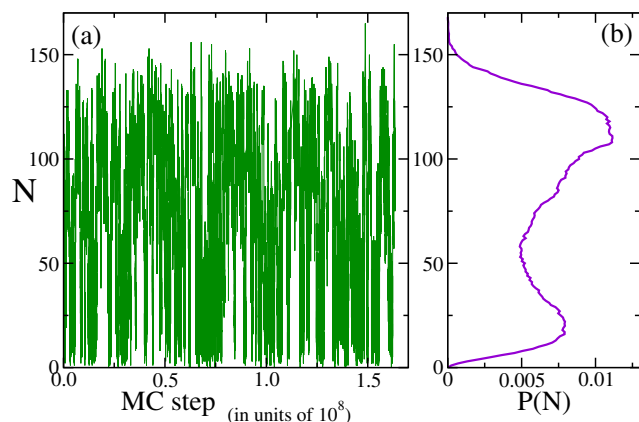
FIG. 2. (Color online) GCMC simulation results for the fluctuations of the number of particles for the largest studied system, i.e., $L=9$, close to the critical point, i.e., $T=0.075$ and $\mu_1=-0.874$ and $\mu_2=-0.358$. Panel (a): the number of particles N vs MC steps for each of the 15 independent realizations of the system (reported in a sequence). Panel (b): the resulting $P(N)$ distribution.

simulated T, μ_1, and μ_2. We tune the chemical potentials of the two species of the mixture in such a way that the proportion of Si and O is well reproduced. We find $T_c=0.0747$, $\mu_1^c=-0.877$, and $\mu_2^c=-0.363$, all in unit of u_0. The average molar fraction of Si, X_{Si}, is equal to ≈ 0.332 at the estimated critical point. The corresponding critical density, in unit of σ^{-3}, is the average of the $P(N)$ distribution and it is found to be $\rho_c=0.0850\pm0.0004$.

To confirm that the critical point is properly located, we also calculate the fluctuation distribution of the ordering operator X at the critical point and compare it to the universal distribution characterizing the Ising class.[14] The ordering operator X of the gas-liquid transition is a linear combination $X \sim \rho + su$, where ρ is the number density, u is the energy density of the system, and s is the field mixing parameter. Exactly at the critical point, fluctuations of X are found to follow the Ising model universal distribution.[14] We implement a fit procedure to estimate the values of s for which the reweighed distribution of N is closest to the known form for Ising-type systems and we find $s=0.458$. Figure 3 shows the
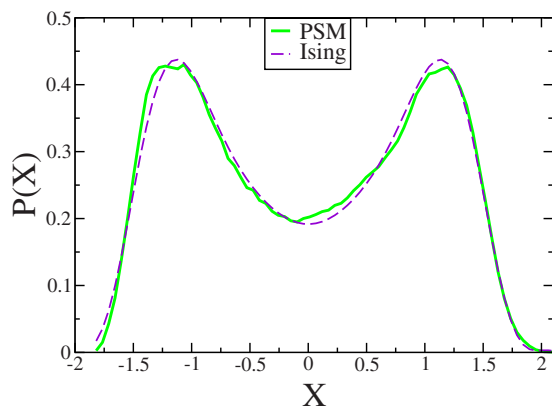

FIG. 3. (Color online) Comparison between the calculated distribution of $X \sim \rho + su$ at the estimated critical temperature T_c and critical chemical potentials μ_1^c and μ_2^c (full line) and the expected distribution (dashed line) for systems at the critical point belonging to the Ising universality class (Ref. 14).

agreement between the PSM critical fluctuation distribution of the order parameter and the Ising one.

We also consider the possible demixing of the binary mixture in phases of different relative compositions of Si and O. In order to evaluate the percentage composition of the two species in both the liquid and the gas phases, we analyze the particle configurations at the critical point, separating the ones with density smaller and larger than ρ_c. We observe that the stoichiometric ratio between Si and O is kept constant in both the dense and diluted phases.

IV. THE THEORY

We complement the numerical study by theoretically estimating the temperature-density location of the gas-liquid critical point. We use two different theoretical approaches: first we use the standard parameter-free Wertheim approach[15,16] and then we develop an interacting bond approach (IBA) by introducing in the Wertheim equation for the bonding probability an appropriate fitting parameter which takes into account the effect of correlation between adjacent bonds.

A. The WT

The Wertheim thermodynamic perturbation theory[15,16] can be applied to all those systems whose interaction potential is composed of a spherical reference repulsion complemented by a directional attraction. Recent applications can be found in Refs. 17–24. For the PSM the reference interaction is the hard core repulsion and the nonspherical attraction is the site-site square well interaction, both described in Sec. II. According to the WT, the free energy per particle $a(\rho,T)$ can be written as the sum of a bonding contribution plus a repulsive one,

$$\beta a(\rho,T) = \beta a^{\text{bond}}(\rho,T) + \beta a^{\text{HS}}(\rho,T). \quad (2)$$

The hard sphere part can be evaluated from the density dependence of the nonadditive hard sphere binary mixture pressure, P^{HS}, as follows:

$$\beta a^{\text{HS}}(\rho,T) = \beta a^{\text{HS}}(\rho_{\text{ref}},T) - \int_{\rho_{\text{ref}}}^{\rho} \beta P^{\text{HS}}(\rho') \frac{d\rho'}{\rho'^2}, \quad (3)$$

where ρ_{ref} is the number density of an arbitrary chosen reference state point. The Helmholtz free energy due to bonding is derived from a summation over certain classes of relevant graphs in the Mayer expansion[25] and it can be simply written as a function of the bond probability p_b as follows:

$$\beta a^{\text{bond}} = \left[f \ln(1-p_b) + \tfrac{1}{2} p_b \right]. \quad (4)$$

Here f is the average system functionality, i.e., two times the ratio between the maximum possible number of bonds in the system and the number of particles. For the present model, the functionality of silicon is $f_{Si}=4$ (while the functionality of oxygen is $f_O=2$) and the molar fraction of silicon is $X_{Si}=1/3$ ($X_O=2/3$). The maximum number of bonds in the
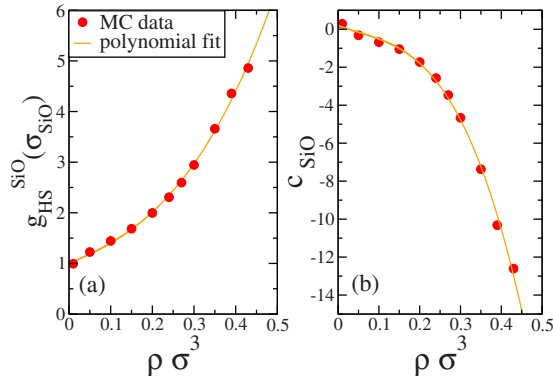
FIG. 4. (Color online) Points are MC data and lines are the corresponding cubic polynomial fits for the contact value [panel (a)] and the slope [panel (b)] of the hard sphere radial distribution function $g_{HS}^{SiO}(r)$. In the linear approximation: $g_{HS}^{SiO}(r) = g_{HS}^{SiO}(\sigma_{SiO}) + c_{SiO}(r - \sigma_{SiO})$, where $g_{HS}^{SiO}(\sigma_{SiO}) = \Sigma_{i=0}^{3} a_i \rho^i$ and $c_{SiO} = \Sigma_{i=0}^{3} b_i \rho^i$, where a_i and b_i are reported in Table I.

system is thus $4N_{Si}$, where N_{Si} is the number of silicon particles, and hence the resulting average functionality of the system is $f = 8/3$.

Since we assume equal reactivity of all the sites, the bonding process can be seen as a chemical reaction between two unsaturated sites in equilibrium with a pair of bonded sites. In this respect, one can write

$$\frac{p_b}{(1-p_b)^2} = \rho\sigma^3 e^{-\beta\mathcal{F}_b}, \tag{5}$$

where $\mathcal{F}_b$ is the site-site bond free energy, i.e., the free energy difference between the bonded and the unbonded states. The WT predicts an expression for $\mathcal{F}_b$ in terms of liquid state correlation functions and spherically averaged Mayer functions. More precisely $\sigma^3 e^{-\beta\mathcal{F}_b} = f/2\Delta$ or, equivalently,

$$\frac{p_b}{(1-p_b)^2} = \rho\frac{f}{2}\Delta, \tag{6}$$

where Δ refers to a single Si–O bond and is defined as an integral, over the range where bonding occurs, of the hard sphere fluid pair correlation function for the Si–O pair, $g_{HS}^{SiO}(r)$, and of the angle-averaged Mayer function for the site-site attraction, i.e.,

$$\Delta = 4\pi \int_{\sigma_{SiO}}^{\sigma_{SiO}+\delta} g_{HS}^{SiO}(r)\langle f_{SiO}(\mathbf{r}, \omega_{Si}, \omega_{O})\rangle_{\omega_{Si}, \omega_{O}} r^2 dr. \tag{7}$$

Here the Mayer function between a Si site and an O site is $f_{SiO}(\mathbf{r}, \omega_{Si}, \omega_{O}) = \exp[-V_{SW}(\mathbf{r}^{SiO})/k_B T] - 1$, where $\mathbf{r}$ and $\mathbf{r}^{SiO}$ are the center-to-center and the site-site distances, respectively. In Eq. (7), $\langle\cdots\rangle_{\omega_{Si}, \omega_{O}}$ represents an angle-average over all orientations of Si and O particles at a fixed relative distance. We note that, since the WT is insensitive to the arrangement of the sites, the number of bonding sites is simply encoded in the factor $f/2$ in front of Δ in Eq. (6), where the factor of 1/2 takes into account that the attractive interaction takes place only between sites of different types.

To determine the bonding contribution to the free energy of the system we need to solve Eq. (7). The Mayer function can be calculated as[26]

$$\langle f_{SiO}(\mathbf{r}, \omega_{Si}, \omega_{O})\rangle_{\omega_{Si}, \omega_{O}} = (e^{\beta u_0} - 1)S(r), \tag{8}$$

where $S(r)$ is the fraction of solid angle available to bonding when two particles are located at relative center-to-center distance r, i.e.,

$$S(r) = \frac{(\delta + \sigma - r)^2(2\delta - \sigma + r)}{6\sigma^2 r}, \tag{9}$$

(where $\sigma_{SiO} = \sigma$). The evaluation of Δ from Eq. (7) thus requires only an expression for $g_{HS}^{SiO}(r)$ for distances smaller than δ. As previously done for the case of PMW,[27] we assume a linear dependence of $g_{HS}^{SiO}(r)$ for r close to σ_{SiO}, i.e.,

$$g_{HS}^{SiO}(r) = g_{HS}^{SiO}(\sigma_{SiO}) + c_{SiO}(r - \sigma_{SiO}), \tag{10}$$

where the density dependence enters in the two parameters: $g_{HS}^{SiO}(\sigma_{SiO})$ (the contact value) and c_{SiO} (the slope). Figure 4 shows the density dependence of $g_{HS}^{SiO}(\sigma_{SiO})$ and c_{SiO} on the MC data and the associated cubic polynomial fits. The resulting fit parameters are reported in Table I. In the low density limit we find the ideal gas value $g_{HS}^{SiO}(r) \approx 1$.

The resulting expression of Δ is

$$\Delta = (e^{\beta u_0} - 1)V_b\chi(\rho), \tag{11}$$

where V_b is the bonding volume in the low density limit,

TABLE I. Parameters of the polynomial fits for (from left to right) the contact value of the hard sphere radial distribution function, the slope of $g_{HS}^{SiO}(r)$ in the linear approximation, the function $\chi(\rho)$ in Eq. (11), the hard sphere pressure of the system [here the value of the second virial coefficient is $B_2^{HS} = 4.976\,28$ from Eq. (15)], and the parameter $\alpha(\rho)$ in Eq. (16). Note that, by definition, the i-coefficient has the dimension of ρ^{-i} in all the columns.

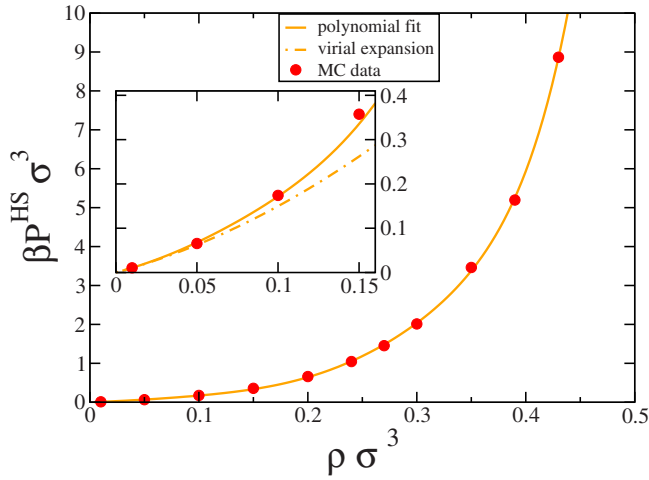|	$g_{HS}^{SiO}(\sigma_{SiO})$	c_{SiO}	χ	βP^{HS}	α
0th	1.0027	0.188 69	1.009 57	0	1.0414
1st	3.4069	−7.766 30	3.124 05	1	−1.23981
2nd	3.7852	25.949 00	4.730 26	B_2^{HS}	−3.9475
3rd	22.375	−183.79	15.681 4	107.392	⋯
4th	⋯	⋯	⋯	−1 820.26	⋯
5th	⋯	⋯	⋯	12 857.5	⋯
6th	⋯	⋯	⋯	−35 514.8	⋯
7th	⋯	⋯	⋯	35 568.2	⋯

FIG. 5. (Color online) Hard sphere pressure as a function of the total number density of the system. Points are MC data and the solid line is the corresponding polynomial fit: $\beta P^{HS} = \sum_{i=0}^{7} c_i \rho^i$, where the coefficients c_i are reported in Table I. The inset shows an enlargement of the low density region and a comparison with the approximation of Eq. (14) (dotted line).

$V_b = 4\pi \int_{\sigma_{SiO}}^{\sigma_{SiO}+\delta} S(r) r^2 dr = 0.000\,524\,15\sigma^3$, and $\chi(\rho)$ incorporates the remaining density dependence of Δ: Upon increasing ρ, the bond probability increases as well due to the structuring associated with the hard sphere excluded volume interactions. We note that the free energy associated with the bonding process can be expressed as a function of the microscopic parameters characterizing the system. More precisely, it is a function of the bonding volume and of an exponential temperature factor as follows:

$$\beta \mathcal{F}_b = -\ln\left[(e^{\beta u_0} - 1)\frac{f}{2}\frac{V_b}{\sigma^3}\chi(\rho)\right]. \quad (12)$$

Once the function Δ is known [Eq. (11)], it is possible to solve Eq. (6) and find $p_b(T,\rho)$, which is the only thermodynamic quantity involved in the bond free energy [see Eq. (4)].

To determine the reference free energy [see Eq. (3)], we numerically evaluate, via MC simulations, the equation of state of the reference nonadditive hard sphere mixture. For hard sphere interactions, the pressure can be calculated from the contact value of the hard sphere radial distribution functions as

$$P_{HS} = \rho k_B T + \frac{2\pi}{3}\rho^2 [X_{Si}X_O \sigma_{SiO}^3 g_{HS}^{SiO}(\sigma_{SiO})$$
$$+ X_O^2 \sigma_{OO}^3 g_{HS}^{OO}(\sigma_{OO}) + X_{Si}^2 \sigma_{SiSi}^3 g_{HS}^{SiSi}(\sigma_{SiSi})]. \quad (13)$$

The resulting pressure is shown in Fig. 5. We also fit the MC data with a polynomial form, whose coefficients are reported in Table I. To improve the quality of the fit we constrain the first two coefficients to the theoretically known low density behavior. Indeed, from the virial expansion we know that in the low density limit the pressure can be expressed as

$$\frac{\beta P^{HS}}{\rho} = 1 + B_2^{HS}\rho. \quad (14)$$

The virial coefficient of a binary mixture is defined as

TABLE II. T_c is the gas-liquid critical temperature and ρ_c is the density of the critical point as estimated from GCMC simulations, the WT, and the IBA.

	$k_B T_c / u_0$	$\rho_c \sigma^3$
MC	0.0747	0.0850
WT	0.0743	0.0151
IBA	0.0749	0.0954

$$B_2(T) = X_{Si}^2 B_2^{SiSi}(T) + X_O^2 B_2^{OO}(T) + 2X_{Si}X_O B_2^{SiO}(T). \quad (15)$$

In the hard sphere limit, we have $B_2^{SiSi} = B_2^{SiO} = 2\pi/3\sigma^3$, $B_2^{OO} = 2\pi/3(1.6\sigma)^3$, and hence $B_2^{HS} = 4.976\,28\sigma^3$.

From the knowledge of the resulting total free energy, it is now possible to locate the position in T and ρ of the gas-liquid critical point by solving the coupled system of equations $(\partial^2 a(T,V)/\partial V^2)_T = 0$ and $(\partial^3 a(T,V)/\partial V^3)_T = 0$. The resulting critical T_c and ρ_c values are reported in Table II. While T_c correctly reproduces the "exact" MC numerical value, the predicted critical density is significantly different.

To pin down the origin of this discrepancy, we compare theoretical and simulation results for the temperature and density dependences of p_b, a key element in the WT [see Eq. (6)]. In this model, p_b provides a measure of the potential energy of the system and can thus be easily compared to the numerical results. In particular the energy per Si particle is simply given by $e^{Si} = -4u_0 p_b$, and hence the system ground state energy (per particle) is $e_{gs}^{Si} = -4u_0$. A comparison between the predicted Wertheim values for $e^{Si}(T,\rho)$ with the available numerical results from Ref. 3 is reported in Fig. 6. The agreement between the theoretical predictions and the numerical results is rather unsatisfactory, especially in comparison with the previously reported studies of models for colloidal patchy particles.[22,23] Even more astonishingly, the disagreement appears to increase in the region of small densities where the theory should, in principle, work better.

B. IBA

To highlight the origin of the disagreement we look more carefully into the ρ and T dependences of p_b. Inspired by the functional form suggested by Eq. (6), we single out the bonding volume contribution [see Eq. (11)], which, according to the WT, should remain constant to the value of $V_b = 0.000\,524\,15\sigma^3$ under the assumption of independent bonds. We define V_b^c, the bonding volume in the presence of bond correlation, as $V_b^c \equiv [p_b/(1-p_b)^2]/[\rho(f/2)(e^{\beta u_0}-1)\chi(\rho)]$. Figure 7 shows that V_b^c departs from the V_b value upon increasing p_b, signaling a reduction in the available bonding volume in the presence of already bonded configurations. This suggests that the bonding volume entering in the chemical equilibrium between bonded and unbonded pairs is a function of the extent of bonding present in the system. Thus, the reason for the failure of the WT in the present model can be ascribed to the fact that the assumption of independent bonding sites is not fully satisfied. This is due to the nonadditivity of the O–O interaction. Indeed, when an O particle is bonded to a Si particle, the very large repulsive diameter determines a reduction in the bonding volume of
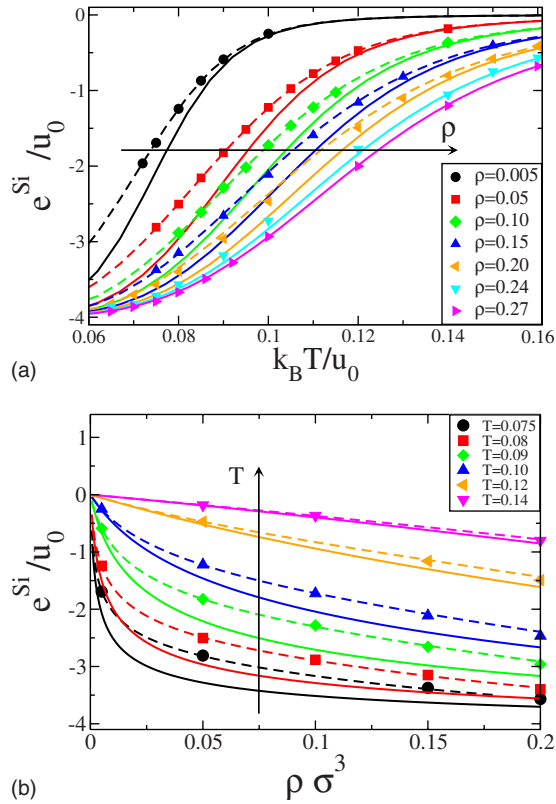
FIG. 6. (Color online) Energy per Si particle as a function of temperature [panel (a)] and density [panel (b)]. Points are numerical results from Ref. 3, solid lines are WT predictions, and dashed lines are IBA predictions.

FIG. 8. (Color online) Oxygen-silicon-oxygen angle vs oxygen-oxygen center-to-center distance for a bonded triplet O–Si–O. Points are all the possible combinations of angles and distances between the two O particles bonded to a Si one. The inner the color layer is, the most probable the bonded configuration is. The (purple) vertical line on the left corresponds to the Si–O hard sphere diameter. The (red) horizontal line represents the cosine of the tetrahedral angle. The (blue) vertical line on the right corresponds to the minimum allowed distance between the oxygen particles, i.e., the hard core O–O diameter 1.6σ. All points with $r_{O-O} < \sigma_{OO} \equiv 1.6\sigma$ represent bonded configurations forbidden by sterical constraints.

the adjacent bonding sites. In this respect, the probability of forming additional bonds is reduced as compared to the one of forming the first bond. Interestingly, it appears that the increase of density compensates this sterically induced bond correlation, resulting in a cancellation of errors and in an optimal performance in density of around $\rho = 0.27$.
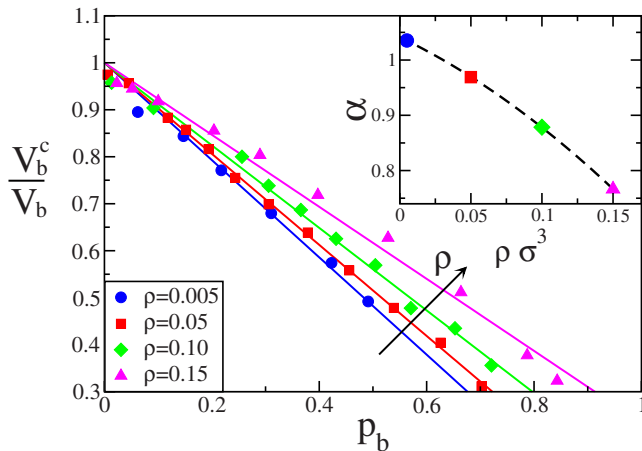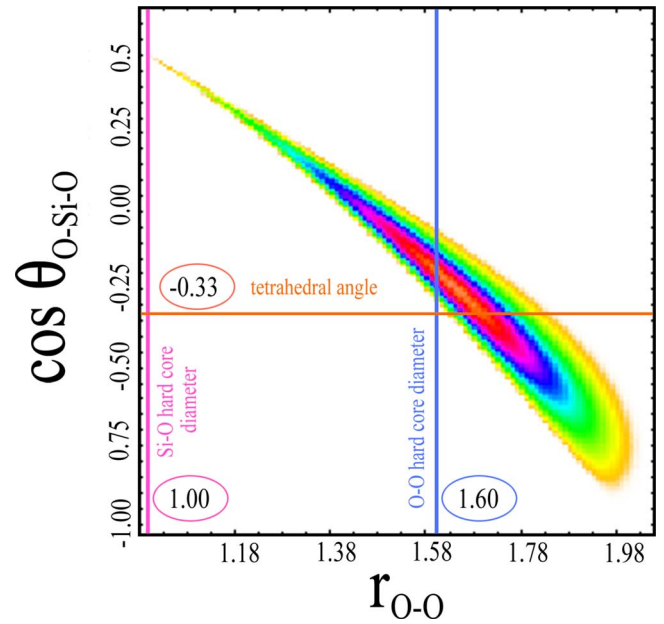
To quantify the correlation between adjacent bonding

FIG. 7. (Color online) Bonding probability dependence of $V_b^c \equiv [p_b/(1-p_b)^2]/[\rho(f/2)(e^{\beta u_0}-1)\chi(\rho)]$. If the WT holds, a plot of V_b^c/V_b should result in a constant value of one. V_b^c shows instead a linear dependence on p_b, reproduced by $V_b^c = 1 - \alpha(\rho)p_b$. Points refer to data from simulations, while lines are linear fits, whose slopes give the density dependence of $\alpha(\rho)$. The inset shows the resulting values of α for the four studied densities and the dotted line is their quadratic fit: $\alpha(\rho) = \Sigma_{i=0}^{2} d_i \rho^i$, where d_i are reported in Table I.

sites we generate, via a MC technique, a large number of configurations ($\sim 10^8$) of three particles, in which two O particles are connected to a central Si particle via bonds. In doing so, we do not account for any interaction between the two O particles. We then evaluate the fraction of these configurations for which the distance between the center of the two O particles is smaller than σ_{OO}. We find that about $\approx 30\%$ of the configurations is forbidden due to sterical constraints, providing a mechanism for decreasing the bond probability upon the presence of pre-existing bonds. The shading of a bonding site by the presence of a nearby bonded site introduces in the system a sort of negative cooperativity which reduces the bonding probability (see Fig. 6). To better visualize the described phenomena, we report in Fig. 8, for each of the generated configuration, the O–Si–O angle versus the corresponding O–O distance r_{O-O}. In this plot, only points with $r_{O-O} \geq \sigma_{OO} \equiv 1.6\sigma$ represent allowed PSM configurations.

In an attempt to cure the WT, we develop a zeroth order theoretical approach in which the interaction between adjacent bonding sites is taken into account via a density dependent parameter, which properly reproduces the observed linear p_b dependence of V_b^c as $V_b^c = 1 - \alpha(\rho)p_b$. In other words, we substitute the independent-bond expression of Eq. (6) by

$$\frac{p_b}{(1-p_b)^2} = \rho\frac{f}{2}\Delta(1 - \alpha(\rho)p_b). \qquad (16)$$

Figure 7 shows a linear relation between V_b^c and p_b, whose slope is density dependent. The resulting linear fit parameters

$\alpha(\rho)$ are shown in the inset of Fig. 7. The density dependence of α can now be conveniently parametrized by a quadratic expression, whose coefficients are reported in Table I. This modification captures the physics of the progressive reduction in the bonding volume on progressive bonding since the term $(1-\alpha(\rho)p_b)$ multiplies the bare bonding volume V_b (contained in Δ). Using the polynomial expression for $\alpha(\rho)$ from Table I, it is possible to solve Eq. (16) and obtain the T and ρ dependences of p_b. The resulting p_b expression does now reproduce, as shown in Fig. 6, quite precisely the bond probability in a large region of T and ρ.

The equivalence between p_b and the potential energy e offers a way to extract, a part from an unknown constant, the density and temperature dependences of the bonding contribution to the free energy. Indeed, the free energy per particle is defined by the standard thermodynamics relation

$$a(\rho, T) = e(\rho, T) - Ts(\rho, T) \tag{17}$$

where $e(\rho, T) = -\frac{4}{3} p_b(\rho, T)$. Choosing a large T_{ref}, so that $s(\rho_{\text{ref}}, T_{\text{ref}})$ coincides with the entropy of the reference non-additive hard sphere binary system, and integrating along a reversible path in the T-ρ plane, $s(\rho, T)$ can be written as

$$s(\rho, T) = s(\rho_{\text{ref}}, T_{\text{ref}}) + \int_{T_{\text{ref}}}^{T} \frac{C_V(\rho, T')}{T'} dT'$$
$$- \int_{\rho_{\text{ref}}}^{\rho} \frac{P^{\text{HS}}(\rho', T_{\text{ref}})}{T_{\text{ref}}} \frac{d\rho'}{\rho'^2}. \tag{18}$$

Here $C_V(\rho, T)$ is the constant volume specific heat and is defined as $C_V(\rho, T) = (\partial e(\rho, T)/\partial T)_\rho$.

Repeating calculations analogous to the one reported in Sec. IV A, we locate the position in T and ρ of the critical point using the derived total free energy density $a(T, \rho)$ expression [Eq. (17)]. The resulting T and ρ critical values, reported in Table II, reproduce accurately the exact numerical data both for T_c and ρ_c.

V. CONCLUSIONS

In this article we report a study of the gas-liquid critical behavior of a simple but powerful primitive patchy model for silica.[1] We determine the location of the gas-liquid critical point in the temperature-density plane by means of extensive GCMC simulations. Figure 9 shows the critical point estimates, reported in this article, within the equilibrium phase diagram of the PSM from Ref. 1. The gas-liquid phase separation region is found to be well inside the fluid-solid coexistence region, confirming that a *stable* liquid phase cannot be observed in this silica model. In other words, the liquid phase is always metastable with respect to the crystalline phase. We thus find a result similar to the case of short-range attractive colloids[4–7] and to the case recently reported for a primitive model for water.[10]

We also compare the exact numerical value and two different theoretical estimates of T_c and ρ_c. We use the standard parameter-free WT[15,16] and an IBA developed to better take into account the peculiarity of PSM. We find that the WT is able to well reproduce T_c, while ρ_c is far from the MC value. We also find a discrepancy between the predicted bonding
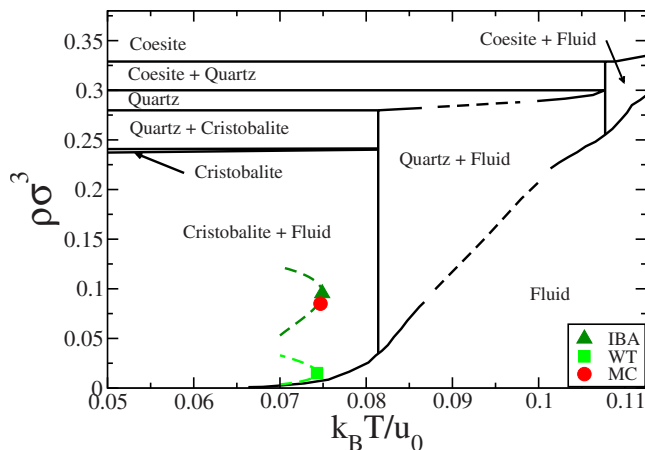

FIG. 9. (Color online) Location of the gas-liquid critical point in the phase diagram of the PSM from Ref. 1. The (red) circle is the exact critical point from MC simulations, the (light green) square is the standard parameter-free WT estimate for T_c and ρ_c, and the (dark green) triangle is the IBA estimate of the critical point. We also report the theoretical spinodal lines [the locus of points such that $(\partial \beta P/\partial V)_T = 0$] close the critical points.

probability and the simulation data: in the studied region of T and ρ the predicted p_b is found to be always larger than the numerical one. Moreover the magnitude of the discrepancy increases upon decreasing the density of the system even in the limit of very low density ($\rho \approx 0.005$) where the WT should work well.

We thus derive the IBA from the Wertheim equation of the chemical equilibrium between bonded and unbonded pairs by introducing an appropriate fitting parameter which takes into account the ρ dependent decrease in p_b. We find that our IBA well predicts the potential energy of the system as well as T_c and ρ_c.

We suggest that the reason of the extra ρ dependence of p_b could be ascribed to the nonadditive interactions of the model. The PSM is indeed a nonadditive binary mixture of silicon and oxygen in a stoichiometric ratio. The large O–O hard core repulsion reduces the number of O–Si–O bonded configurations. The percentage of O–Si–O configurations, which are not allowed to be bonded due to the O–O repulsion, is found to be $\approx 30\%$. The bonding volume is thus dependent on the extent of bonding already present in the system. In other words, the nonadditivity of the mixture introduces a three-particle interaction in the bonding process. The bonding sites are no longer independent of each other since the presence of a bond hinders the formation of a second additional bond on the same particle. The interaction between adjacent sites can be seen as a sort of negative cooperativity since the probability of forming additional bonds is less than the probability of forming the first Si–O bond.

In summary, the present study confirm that PSM does not show an equilibrium liquid phase but only a metastable form of it, as in spherically interacting short-ranged potentials. It also provides a detailed frame for testing theories for (anti)correlated bond formation,[28,29] as well as suggests modifications of the original WT to account for bond correlations.

ACKNOWLEDGMENTS

[1] M. H. Ford, S. M. Auerbach, and P. A. Monson, J. Chem. Phys. **121**, 8415 (2004).

[2] M. H. Ford, S. M. Auerbach, and P. A. Monson, J. Chem. Phys. **126**, 144701 (2007).

[3] C. De Michele, P. Tartaglia, and F. Sciortino, J. Chem. Phys. **125**, 204710 (2006).

[4] C. F. Tejero, A. Daanoun, H. N. W. Lekkerkerker, and M. Baus, Phys. Rev. Lett. **73**, 752 (1994).

[5] G. A. Vliegenthart and H. N. W. Lekkerkerker, J. Chem. Phys. **112**, 5364 (2000).

[6] H. Liu, S. Garde, and S. Kumar, J. Chem. Phys. **123**, 174505 (2005).

[7] D. L. Pagan and J. D. Gunton, J. Chem. Phys. **122**, 184515 (2005).

[8] R. Piazza, Curr. Opin. Colloid Interface Sci. **5**, 38 (2000).

[9] M. Muschol and F. Rosenberger, J. Chem. Phys. **103**, 10424 (1995).

[10] F. Romano, P. Tartaglia, and F. Sciortino, J. Phys.: Condens. Matter **19**, 322101 (2007).

[11] A. M. Ferrenberg and R. H. Swendsen, Phys. Rev. Lett. **61**, 2635 (1988).

[12] J. B. Caballero, A. M. Puertas, A. Fernández-Barbero, and F. J. de las Nieves, J. Chem. Phys. **121**, 2428 (2004).

[13] R. L. C. Vink and J. Horbach, J. Chem. Phys. **121**, 3253 (2004).

[14] N. B. Wilding, J. Phys.: Condens. Matter **9**, 585 (1997).

[15] M. Wertheim, J. Stat. Phys. **35**, 19 (1984); **35**, 35 (1984).

[16] M. Wertheim, J. Stat. Phys. **42**, 459 (1986); **42**, 477 (1986).

[17] R. Melnyk, F. Moucka, and I. Nezbeda, J. Chem. Phys. **127**, 094510 (2007).

[18] J. Jirsák and I. Nezbeda, J. Chem. Phys. **127**, 124508 (2007).

[19] A. Gil-Villegas, A. Galindo, P. J. Whitehead, S. J. Mills, G. Jackson, and A. N. Burgess, J. Chem. Phys. **106**, 4168 (1997).

[20] A. Galindo, A. Gil-Villegas, G. Jackson, and A. N. Burgess, J. Phys. Chem. **103**, 10272 (1999).

[21] E. Bianchi, J. Largo, P. Tartaglia, E. Zaccarelli, and F. Sciortino, Phys. Rev. Lett. **97**, 168301 (2006).

[22] F. Sciortino, E. Bianchi, J. F. Douglas, and P. Tartaglia, J. Chem. Phys. **126**, 194903 (2007).

[23] E. Bianchi, P. Tartaglia, E. La Nave, and F. Sciortino, J. Phys. Chem. B **111**, 11765 (2007).

[24] E. Bianchi, P. Tartaglia, E. Zaccarelli, and F. Sciortino, J. Chem. Phys. **128**, 144504 (2008).

[25] J. P. Hansen and I. R. McDonald, *Theory of Simple Liquids*, 3rd ed. (Academic, New York, 2006).

[26] M. Wertheim, J. Chem. Phys. **85**, 2929 (1986).

[27] C. De Michele, S. Gabrielli, P. Tartaglia, and F. Sciortino, J. Phys. Chem. B **110**, 8064 (2006).

[28] R. P. Sear and J. G. Jackson, J. Chem. Phys. **105**, 1113 (1996).

[29] J. F. Douglas, J. Dudowicz, and K. F. Freed, J. Chem. Phys. **128**, 224901 (2008).